

Electro-optic effect of graded-pitch chiral photonic structures under oblique illuminationLaura O. Palomares * and J. Adrian Reyes †*Física Química, Instituto de Física, Universidad Nacional Autónoma de México Apartado Postal 20-364, C.P. 01000, Ciudad de México, Mexico*

(Received 25 March 2020; accepted 23 June 2021; published 19 July 2021)

We studied theoretically optical spectra when circularly polarized light obliquely impinges on a slab of a chiral photonic structure with linearly and uniformly spatially varying pitch. The material that we considered locally has a $42m$ point-group symmetry and presents Pockels effect, hence, we controlled optical spectra by a low frequency (DC) electric field applied along the nonhomogeneity axis. The spectra display a Bragg-type broadband, where the edge wavelengths of the photonic band are expressed in terms of the medium parameters and the external electric-field magnitude. This allows us to select the region of the electromagnetic spectrum, where the band could become as broad as we choose. We studied three samples with iridescent, silver, and golden colors due to their reflection properties. We observed an enhancement as well as a broadening of the optical band by the application of the electric field. We found that, under certain conditions, when the optical band is practically absent, a very broad band could be created (comparable to the whole visible spectrum) when a DC electric field is applied. This is the result of electro-optic contributions in the permittivity tensor elements, which give rise to a tremendous increase in both the rotatory power and dichroism. Therefore, these media could be used as electrically controlled broadband frequency and polarization filters. Moreover, we observed the usual blueshift of the band as the incidence angle of light increases and an asymmetry in the reflection band amplitude as the incidence angle of the light increases, depending on whether the pitch increases or decreases and the pitch gradient; which endows the sample with different reflection colors for different gradients and incidence angles of the light. The asymmetry in the reflection band vanishes as the magnitude of the electric field increases.

DOI: [10.1103/PhysRevA.104.013519](https://doi.org/10.1103/PhysRevA.104.013519)**I. INTRODUCTION**

Chiral photonic structures usually present circular Bragg phenomenon [1–3], where a co-handed circularly polarized plane wave, impinging normally, is highly reflected in a certain wavelength regime, whereas a similar wave of the contrary handedness is extremely transmitted; which made them frequency and polarization filters.

Chiral structures with a constant pitch have been extensively studied due to their technological applications. However, in this study we are concerned with structurally chiral media (SCMs) with spatially varying pitch, which are ubiquitous in nature: they appear especially in the exoskeletons of crustaceans and in the cuticles of insects and beetles. The beautiful colors that are observed in some of these living beings are the result of a chiral structure in their most external layers, giving rise to reflection at certain wavelengths. For instance, iridescent colors are due to reflection in either different or in broad regions of the visible spectrum, while the silver color is due to reflection in a wider region than the visible spectrum; such that the human eye is unable to perceive iridescence [4–14]. Indeed, the graded pitch profiles and effective refractive indexes of some beetles have been recently determined through nonlinear regression analysis of

the experimental Mueller matrix by using a cuticle model based on twisted biaxial dielectric slices [15,16].

Different pitch gradients result in different reflection spectra; for instance, a uniform or linear gradient produces a broadening in the wavelength region of the reflection band, and it is broader as the difference between the initial and final pitch of the structure increases; such that this band can even be broader than the entire visible spectrum. Meanwhile, the repetition of a linear gradient in layers yields reflection in different narrow regions of the electromagnetic spectrum, where a few of the reflection bands can remain in the visible spectrum [17]. Continuously tunable and bandwidth-variable optical notch and band-pass filters were created by using a liquid crystal wedge cell with a continuous-pitch gradient. The band wavelength position can be spatially tuned from 470 to 1000 nm [18]. Also, dye-doped polymer-stabilized cholesteric liquid crystals with negative dielectric anisotropy were fabricated, and mirrorless lasing with an electrically tunable wavelength was successfully achieved. Unlike conventional liquid-crystal lasers, the proposed laser aided in tuning the emission wavelength through controlling the reflection bandwidth based on gradient pitch distribution [19]. Moreover, the reflection band of this type of material has been broadened by applying DC electric fields, which is caused by a pitch gradient that originates in turn by the motion of the polymer backbone [19].

Since some years ago, an important effort has been ongoing for developing efficient methods to produce cholesteric structures with spatially varying pitch, for instance, by thermal processing, by diffusing chiral nematic liquid crystals

*lpaloma_quark@yahoo.com.mx

†adrian@fisica.unam.mx

in silica aerogel, or by physical vapor deposition [2,20–24]. Nowadays, a great deal of interest focuses on designing, based on diverse mechanisms, photonic broadband gaps by means of graded-pitch cholesteric liquid crystals, which have been extensively studied, fabricated, and applied in various contexts [25]. For instance, a humidity-gated temperature-responsive infrared reflective and reversible broadband photonic coating with potential application for smart windows in high-humidity environments has been reported in Ref. [26]. Also, a laser which is aided in tuning the emission wavelength through controlling the reflection bandwidth based on gradient-pitch distribution was achieved by dye-doping polymer-stabilized cholesteric liquid crystals with negative dielectric anisotropy [26]. Besides, chiral nematic liquid crystal slabs with helical order that varies in three dimensions were constructed, namely, gradient-pitch cholesterics endowed with in-plane space-variant angular positioning of the supramolecular helix [27]. Finally, an interesting method for fabricating helical structures with different pitches in order to broaden the reflection band, was managed by controlling the UV-induced polymerization by varying the distance between UV lamp and sample cell, which affects the polymerization rate and leads to the formation of imprinted chiral structures [28].

The electro-optic effect has also been extensively studied in SCMs of constant pitch, where the broadening and enhancement of the Bragg band has been observed [19,24–29]. Here we presented a theoretical study of the electro-optic effect in photonic chiral media with linear pitch gradient and uniformly varying pitch, where a Bragg-type broadband has been produced [17].

In this context, we consider that the appropriate method, to obtain the chiral media with the pitch gradients we propose, is the physical vapor deposition in which a vaporized birefringent solid is gradually deposited over a uniformly rotating substrate to form a helical structure which is similar to a cholesteric liquid crystal. However, the angular velocity of the rotating substrate has to be varied accordingly with the required pitch gradients, instead of keeping it simply constant; the result is a chiral sculptured thin film (CSTF) [2,24] with spatially linear varying pitch. Here, we consider this method to obtain the desired chiral structure, although it is not restricted to this method.

We calculate the circularly copolarized and cross-polarized optical spectra without and with a low frequency (DC) electric field applied along the nonhomogeneity axis, when light obliquely impinges on a slab of structurally chiral medium with a linear or uniformly varying pitch. Based on the electro-optical effect, induced by the externally applied field in the chiral medium, we expect that the magnitude of the optical activity and circular dichroism grow; and in turn, the optical discriminatory band gap broadens. The outline of our paper is the following: in Sec. II we discuss the basic equations. In Sec. III we present with detail our results and discussion. In Sec. IV we finally address our conclusions.

II. MODEL AND BASIC EQUATIONS

We shall analyze the propagation of electromagnetic waves with arbitrary incidence angle, lying in the xy plane of a system formed by a slab of a SCM whose pitch is spatially

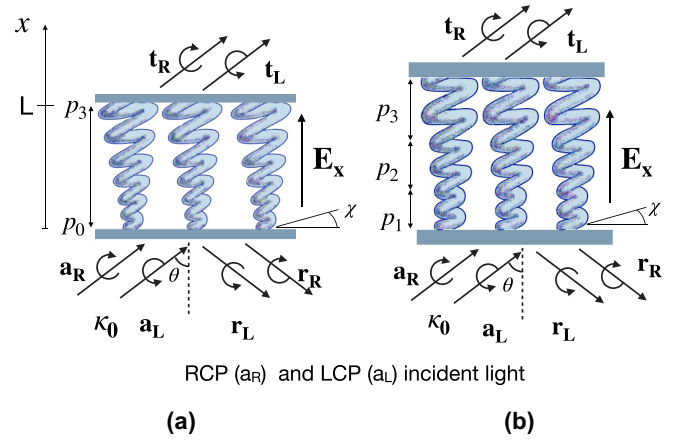


FIG. 1. Obliquely incident light impinges on a SCM with (a) linearly and (b) uniformly spatial varying pitch along the non-homogeneity axis, x axis, where a low-frequency (DC) electric field, $\mathbf{E}_x = E_x \hat{x}$, is applied along the x axis. L is the thickness of the sample and χ is the tilt of the chiral structure. A local structural period is defined as a length along the nonhomogeneity axis, where the director rotates a full turn. (a) The pitch linearly increases (decreases) in every point of the sample with a constant change rate δ from an initial pitch $p_i = p_0$ to a final pitch p_f . The pitch at each point of the sample is $p(x) = p_0 + \delta x$ and the pitch at the end of the j period is $p_j = \frac{p_0}{(1-\delta)^j}$, $j = 1, 2, \dots$, where p_0 and δ are given values. (b) The pitch value is constant in each local structural period and it uniformly increases (decreases) in subsequent periods in the SCM. The pitch value in the first period is p_1 , and, $p_j = p_1 + \delta(j - 1)$, in the j period, where δ is the constant change rate of the pitch value and $j = 1, 2, \dots$.

varying restricted by the planes $x = 0$ and $x = L$ (see Fig. 1). This artificial material can be experimentally built in the same way as a CSTF, whose production process is thoroughly explained elsewhere [2,24].

We take the x direction parallel to helical axis of the structure. In the following discussion we explain a matrix approach to formulate the boundary-value problem which should be solved in order to obtain the reflection and transmission coefficients.

A. Matrix formulation

The propagation of optical waves by a SCM, we study here, is ruled by the Maxwell curl equations and their respective constitutive equations [30]. These equations can be settled (in Gaussian units), for a nonmagnetic medium, in the following form:

$$\frac{\partial \psi(x)}{\partial x} = ik_0 \mathbf{A}(x) \cdot \psi(x), \quad (1)$$

where we have introduced the time-harmonic transversal four-component vector

$$\begin{aligned} \Psi(x, y, z, t) &\equiv \psi(x) \exp[i(k_y y + k_z z) - i\omega t] \\ &= (e_y(x), e_z(x), h_y(x), h_z(x)) \exp[i(k_y y + k_z z) - i\omega t], \end{aligned} \quad (2)$$

and $k_0 = \omega/c$ is the wave number in free space, c stands for the speed of light in vacuum, ω the angular frequency

of the propagating wave and $\mathbf{k}_0 = (k_x, k_y, k_z) = k_0(\cos(\theta), \sin(\theta), 0)$ is the wave vector of the electromagnetic and the angle of incidence of the light is θ ; $e_y(x)$, $e_z(x)$, $h_y(x)$, and

$h_z(x)$ are the transverse components of the electric and magnetic fields, respectively. In Eq. (1), the 4×4 matrix $\mathbf{A}(x)$ is defined as

$$\mathbf{A}(x) = \begin{pmatrix} -\frac{k_y \epsilon_{xy}(x)}{k_0 \epsilon_{xx}(x)} & -\frac{k_y \epsilon_{xz}(x)}{k_0 \epsilon_{xx}(x)} & 0 & 1 - \frac{k_y^2}{k_0^2 \epsilon_{xx}(x)} \\ 0 & 0 & -1 & 0 \\ \frac{\epsilon_{zx}(x) \epsilon_{xy}(x)}{\epsilon_{xx}(x)} - \epsilon_{zy}(x) & \frac{\epsilon_{zx}(x) \epsilon_{xz}(x)}{\epsilon_{xx}(x)} - \epsilon_{zz}(x) + \frac{k_y^2}{k_0^2} & 0 & \frac{k_y \epsilon_{zx}(x)}{k_0 \epsilon_{xx}(x)} \\ \epsilon_{yy}(x) - \frac{\epsilon_{yx}(x) \epsilon_{xy}(x)}{\epsilon_{xx}(x)} & \epsilon_{yz}(x) - \frac{\epsilon_{yx}(x) \epsilon_{xz}(x)}{\epsilon_{xx}(x)} & 0 & -\frac{k_y \epsilon_{yx}(x)}{k_0 \epsilon_{xx}(x)} \end{pmatrix}. \quad (3)$$

Here $\epsilon_{ij}(x)$ ($i, j = x, y, z$) represent the elements of dielectric tensor whose expressions for a material with the point-group symmetry $42m$, which exhibits the Pockels effect under the presence of an externally imposed low-frequency (DC) electric field, $\mathbf{E}_x = E_x \hat{x}$, applied along the nonhomogeneity axis are given [29,31] by

$$\begin{aligned} \epsilon_{xx} &= \epsilon_1 \cos^2(\chi) + \epsilon_3 \sin^2(\chi), \\ \epsilon_{yy} &= \epsilon_1 \cos^2(qx) + \sin^2(qx)[\epsilon_1 \sin^2(\chi) + \epsilon_3 \cos^2(\chi)] + \epsilon_1 E_x [\epsilon_3 r_{41} \cos^2(\chi) - \epsilon_1 r_{63} \sin^2(\chi)] \sin(2qx), \\ \epsilon_{zz} &= \epsilon_1 \sin^2(qx) + \cos^2(qx)[\epsilon_1 \sin^2(\chi) + \epsilon_3 \cos^2(\chi)] + \epsilon_1 E_x [\epsilon_1 r_{63} \sin^2(\chi) - \epsilon_3 r_{41} \cos^2(\chi)] \sin(2qx), \\ \epsilon_{xy} &= \epsilon_{yx} = (\epsilon_1 - \epsilon_3) \sin(qx) \sin(2\chi)/2 - \epsilon_1 E_x (\epsilon_1 r_{63} + \epsilon_3 r_{41}) \cos(qx) \cos(\chi) \sin(\chi), \\ \epsilon_{xz} &= \epsilon_{zx} = -(\epsilon_1 - \epsilon_3) \cos(qx) \sin(2\chi)/2 - \epsilon_1 E_x (\epsilon_1 r_{63} + \epsilon_3 r_{41}) \sin(qx) \cos(\chi) \sin(\chi), \\ \epsilon_{yz} &= \epsilon_{zy} = (\epsilon_1 - \epsilon_3) \sin(2qx) \cos^2(\chi)/2 + \epsilon_1 E_x [\epsilon_1 r_{63} \sin^2(\chi) - \epsilon_3 r_{41} \cos^2(\chi)] \cos(2qx), \end{aligned} \quad (4)$$

where ϵ_1 and ϵ_3 are the elements of the local uniaxial dielectric tensor and are the permittivities in the principal Cartesian coordinate system with axes labeled 1, 2, and 3. The 1 axis, which is known as the distinguished axis, makes a tilt angle χ with respect to the y axis. Finally, the pitch is denoted by p and is related to the helical wave number by $q = 2\pi/p$. These expressions exhibit how the external DC field modifies the dielectric permittivity ellipsoid of a helical medium susceptible to the Pockels effect by means of the electro-optic coefficients r_{ij} . Inserting these element of the dielectric tensor into Eq. (1) gives rise to the governing differential equations for the four transverse components of the electromagnetic wave field.

In what follows we shall discuss some of the optical properties of a SCM for normal incidence. Indeed, when electromagnetic wave propagation in the SCM occurs parallel to the axis of structural chirality; a special case amenable to algebraic analysis emerges.

B. Optical activity, center wavelength and bandwidth for a SCM with an applied low-frequency (DC) electric field

In the particular case of normal incidence, Eq. (1) was solved analytically in Ref. [29] by applying a Osssen transformation defined by

$$\psi'(x) = R(x)\psi(x), \quad (5)$$

where R is given by the expression

$$R(x) = \begin{pmatrix} \cos qx & \sin qx & 0 & 0 \\ -\sin qx & \cos qx & 0 & 0 \\ 0 & 0 & \cos qx & \sin qx \\ 0 & 0 & -\sin qx & \cos qx \end{pmatrix}, \quad (6)$$

which performs the simultaneous rotation of both the electric and magnetic field in the transverse plane. This operation

amounts to going from linearly polarized modes to circularly polarized modes, in which the right- and left-circularly polarized modes are delayed by the phases $-iqx$ and iqx , respectively [18]. Once using this transformation and setting $k_y = 0$, Eq. (1) can be expressed as

$$\frac{d\psi'(x)}{dx} = iA_{ax}\psi'(x), \quad (7)$$

where

$$A_{ax} = \begin{pmatrix} 0 & -iq & 0 & \mu\omega \\ iq & 0 & -\mu\omega & 0 \\ -\omega\epsilon_E/c^2 & -\omega\epsilon_1/c^2 & 0 & -iq \\ \omega\epsilon_D/c^2 & \omega\epsilon_E/c^2 & iq & 0 \end{pmatrix}, \quad (8)$$

$$\epsilon_D = \frac{\epsilon_1 \epsilon_3}{\epsilon_1 \cos^2(\chi) + \epsilon_3 \sin^2(\chi)}, \quad (9)$$

and

$$\epsilon_E = E_x \epsilon_1 \epsilon_D [r_{41} \cos^2(\chi) - r_{63} \sin^2(\chi)]. \quad (10)$$

Since A_{ax} is a matrix whose elements are constants, Eq. (7) can be solved by searching its eigenvectors $\bar{\psi}_j$ and eigenvalues l_j ; that is, we take

$$\psi'(x) = \bar{\psi}_j \exp(il_j x), \quad (11)$$

which yields $(A_{ax} - l_j I_4)\bar{\psi}_j = 0$, where I_4 is 4×4 identity matrix and whose nontrivial solution are given by the secular equation

$$\begin{aligned} \text{Det}(A_{ax} - l_j I_4) &= l^4 - l^2(k_0^2 \epsilon_1 + k_0^2 \epsilon_D + 2q^2) \\ &\quad + k_0^4 (\epsilon_1 \epsilon_D - \epsilon_E^2) \\ &\quad - k_0^2 (q^2 \epsilon_1 + q^2 \epsilon_D) + q^4 = 0. \end{aligned} \quad (12)$$

Thus, solving this equation we get that the four eigenvalues can be written as

$$l_1 = -l_3 = \sqrt{k_0^2 S + q^2 + k_0 \sqrt{k_0^2 (a^2 + \epsilon_E^2) + 4q^2 S}}, \quad (13)$$

$$l_2 = -l_4 = \sqrt{k_0^2 S + q^2 - k_0 \sqrt{k_0^2 (a^2 + \epsilon_E^2) + 4q^2 S}}, \quad (14)$$

where $k_0 = \omega_0/c$ and we have introduced the average $S = (\epsilon_1 + \epsilon_D)/2$, and contrast $a = (\epsilon_1 - \epsilon_D)/2$ of permittivities. Then the rotatory power or optical activity of the material Υ can be analytically derived by taking the phase difference between two forward (backward) modes; that is,

$$\Upsilon/d = l_1 - q - (l_2 + q). \quad (15)$$

Υ/d is the rotatory power per unit of length, where d is the thickness of the sample, and we have included the additional delays $\{-q, q\}$ on each mode originated by the Oseen transformation, as commented above. The exact expression for Υ is obtained after substitution of the foregoing formulas for l_1 and l_2 ; nevertheless, because a is usually a small quantity, it is customary to calculate an expression for Υ up to first order in this parameter. Notice, however, that for our case the difference involved in the definition of Υ is also depending on ϵ_E which in turn is a function of the external DC electric field. Hence, in order to perform the mentioned expansion, we assume that ϵ_E is small, which gives

$$\begin{aligned} \Upsilon/d &= \frac{q(a^2 + \epsilon_E^2)}{4(\lambda')^2 S^2 [1 - (\lambda')^2]} \\ &\quad - \frac{q(a^2 + \epsilon_E^2)^2 [1 - 5(\lambda')^2]}{64(\lambda')^4 S^4 [1 - (\lambda')^2]^3} + O(a^2 + \epsilon_E^2)^3 + \dots, \end{aligned} \quad (16)$$

where we have replaced $q/(\sqrt{S}k_0) = \lambda'$ with $k_0 = 2\pi/\lambda$, the reduced wavelength per helical-pitch unit is $\lambda' = \lambda/(p\sqrt{S})$. This expression is consistent with the one derived by De Vries [1], when we keep up to second order in a and turn off the DC field, $\epsilon_E = 0$. For this case, if we take a structure whose pitch is $p \approx 300$ nm and take typical values for ϵ_1 and ϵ_3 , we find that $(a/S)^2 \approx 10^{-3}$ and then $\Upsilon/d \approx 10^3$ deg/cm, which is a gigantic optical activity being striking different from that of an isotropic liquid; nevertheless, typical for a cholesteric-like structure. However, when taking into account the DC electric field, the rotatory power should be even larger because its contribution is quadratic. As can be seen, the external electric field contributes greatly to increase the optical activity of the helical structure.

On the other hand, expressions for the band edges of the SCM of the partial reflection band can be obtained from Eq. (14) by looking for the frequencies where this mode is no longer real ($l_2 = 0$). Once having these frequencies, we get their respective wavelengths and from them we can find formulas for the center wavelength $\lambda_{0_{p=cte}}^{\text{Br}}$ and bandwidth $\Delta\lambda_{0_{p=cte}}^{\text{Br}}$, for a SCM with a constant pitch and a low-frequency (DC) electric field $\mathbf{E}_x = E_x \hat{x}$ applied along the nonhomogeneity

axis \hat{x} [29]. These are given by

$$\lambda_{0_{p=cte}}^{\text{Br}} = \frac{p}{2} (\sqrt{\epsilon_{B\xi}} + \sqrt{\epsilon_{D\xi}}), \quad (17)$$

$$\Delta\lambda_{0_{p=cte}}^{\text{Br}} = p |(\sqrt{\epsilon_{B\xi}} - \sqrt{\epsilon_{D\xi}})|, \quad (18)$$

where for a local point-group symmetry $\bar{4}2m$ with electro-optic coefficients r_{41} and r_{63} (all other electro-optic coefficients are zero, $r_{JK} = 0$, $J = 1, 2, \dots, 6$ and $K = 1, 2, 3$),

$$\epsilon_{B\xi} = \frac{1}{2} \left[\epsilon_1 + \epsilon_D + \frac{(\epsilon_1 - \epsilon_D)^2 + 4\epsilon_E^2}{\epsilon_1 - \epsilon_D} \cos(2\xi) \right], \quad (19)$$

$$\epsilon_{D\xi} = \frac{1}{2} \left[\epsilon_1 + \epsilon_D - \frac{(\epsilon_1 - \epsilon_D)^2 + 4\epsilon_E^2}{\epsilon_1 - \epsilon_D} \cos(2\xi) \right], \quad (20)$$

$$\xi = \frac{1}{2} \tan^{-1} \left(\frac{2\epsilon_E}{\epsilon_D - \epsilon_1} \right). \quad (21)$$

Next we analyze structures possessing a variable pitch with the help of the results and expressions summarized in this section.

C. Boundary conditions transfer matrix and numerical procedure for SCM with variable pitch

We state formally the general solution of Eq. (1) for a wave propagating from $x = 0$ to $x = L$ in the following form:

$$\begin{aligned} \psi(L) &= \mathbf{M} \cdot \psi(0) \\ &\equiv \exp \left[ik_0 \int_0^L \mathbf{A}(x') dx' \right] \cdot \psi(0), \end{aligned} \quad (22)$$

where \mathbf{M} stands for the transfer matrix, which allows us to obtain the wave vector ψ at the left side of the photonic structure departing from the corresponding wave vector at the right side. In this work, we compute the matrix \mathbf{M} by assuming that our incident wave is expressed in terms of right- and left-circularly polarized (RCP and LCP, respectively) fields. The square of the absolute value of the elements of transfer matrix is to be used to calculate the corresponding transmittances and reflectances.

The numerical integration of Eq. (22) was performed by means of the piecewise uniform approximation of the transfer matrix \mathbf{M} , over the whole SCM slab. As can be observed from Eq. (3) the elements of the matrix \mathbf{A} are explicit functions of x . However, we can divide the whole sample in many thin slices parallel to the plane boundaries, each of them characterized with homogeneous and anisotropic optical parameters. As we increased the number of slices for a given sample, the thickness of each slice diminishes so that the variation with x of its elements is very small and it can be neglected. The matrix \mathbf{M} can be recovered by multiplying iteratively the matrix associated with each of the many thin layers from $x = 0$ to $x = L$. The accuracy of the method grows by enlarging the number of slices until certain critical size which is monitored by checking the convergence in each calculation.

Because a SCM with variable pitch is no more a one-dimensional (1D) period system, we need to define a locally structural period as the distance along the helical axis (x axis), for which the director rotates a complete turn (2π). From now on, the pitch, $p = 2\pi/q$ is varying. Whether the pitch p is

constant in the whole structure, the helical wave number q is constant, and the structural period is the pitch; differently, when the pitch value spatially varies, we have a different value for the period after each turn. Hence, the j turn is referred to as the j period.

With this convention, the integration limits of the numerical integration are to be chosen by complete turns of the director (integer multiples of 2π). Therefore, the varying period can be specified in terms of the initial pitch value p_0 , the rate of change of the pitch value, δ , and the particular period number, j . Complementary, if the pitch depends linearly on the x coordinate, with parameters δ and j , $p = p(x)$, and $q = \frac{2\pi}{p(x)}$. For our research, we assume the following two distinct models for representing a SCM with pitch gradients:

(a) SCM with linear pitch gradient: This model embodies a spatially continuous (linear) variation of the pitch from the initial value p_0 to the final local structural period p_n of the SCM, where n is the number of turns in the slab. The pitch in the j period changes linearly depending on the x coordinate as $p_j(x) = p_{j-1} + \delta x$, where the initial pitch of the j period is $p_{j-1} = \frac{p_0}{(1-\delta)^{j-1}}$ and the final pitch is $p_j = \frac{p_0}{(1-\delta)^j}$, for a given pitch rate of change, δ , and initial pitch, p_0 , with $j = 1, 2, \dots, n$; regarding a sample with n periods, where the length of the j period is $p_j - p_{j-1}$. As a consequence, the final pitch for each turn is determined in terms of the initial pitch p_0 , the pitch rate of change δ , and j .

(b) SCM with uniformly spatial varying pitch: The pitch is constant within each turn but it changes with a constant pitch rate of change after the director has completed a whole turn, see Fig. 1(b). There, for the j period, the pitch value is $p_j = p_1 + \delta(j-1)$, where p_1 is the pitch value in the first period of the chiral structure, δ is the pitch rate of change and $j = 1, 2, 3, \dots, n$, with n being the number of periods in the SCM.

In a previous study [17], we found numerically that, for normal incidence of light on a structurally chiral medium with either linearly or uniformly varying pitch, with initial p_i and final p_f pitch in the structure, the low and high edges of the Bragg regime are approximately equal to the low edge of a SCM with constant pitch p_i and to the high edge of a SCM with constant pitch p_f , respectively. Therefore, by generalizing this result, for normal incidence on a SCM with either linear or uniformly varying pitch, the center wavelength of the Bragg-type regime is approximately given by

$$\lambda_0 = \frac{1}{2}(p_{i(f)}\sqrt{\epsilon_{D\xi}} + p_{f(i)}\sqrt{\epsilon_{B\xi}}), \quad (23)$$

and the corresponding full-width-at-half-maximum (FWHM) bandwidth is

$$\Delta\lambda_0 = p_{f(i)}\sqrt{\epsilon_{B\xi}} - p_{i(f)}\sqrt{\epsilon_{D\xi}}. \quad (24)$$

Hence, the edges of the optical band are

$$\lambda_- = p_{i(f)}\sqrt{\epsilon_{D\xi}}, \quad (25)$$

$$\lambda_+ = p_{f(i)}\sqrt{\epsilon_{B\xi}}, \quad (26)$$

where the sign minus (plus) in the subscript is applied for the edge bandwidth at shorter (longer) wavelengths. In the subscripts of Eqs. (23)–(26), the letter outside (inside) the parentheses is used when $p_f > p_i$ ($p_i > p_f$). Also, the circular optical activity can be generalized for variable-pitch

structures in the following way

$$\frac{\gamma}{2\pi d} = \frac{(a^2 + \epsilon_E^2)}{4\lambda_0\tilde{\lambda}^2 S^2(1 - \tilde{\lambda}^2)}, \quad (27)$$

where $\tilde{\lambda} = \lambda/\lambda_0$. This means that a small pitch gradient δ disturbs adiabatically the whole structure in such way that the graded pitch chiral medium behaves locally as an ordinary constant-pitch chiral medium.

III. RESULTS AND DISCUSSION

We considered circularly polarized light obliquely impinging on a right-handed structurally chiral medium with spatially varying pitch and the $\bar{4}2m$ point-group symmetry. The material is ammonium dihydrogen phosphate (ADP, $\text{NH}_4\text{H}_2\text{PO}_4$). It presents the Pockels effect, which allows us to modify the refractive indexes by an external low-frequency (DC) electric field applied to the chiral medium along the non-homogeneity axis. The material refractive indexes are $n_1 = 1.530$, $n_3 = 1.483$ ($\epsilon_1 = n_1^2$, $\epsilon_3 = n_3^2$), the electro-optic coefficients are $r_{41} = 24.5$ pm/V and $r_{63} = 8.5$ pm/V, all other electro-optic coefficients are zero, $r_{JK} = 0$, $J = 1, 2, \dots, 6$ and $K = 1, 2, 3$ [32]; the tilt of the chiral structure is $\chi = \pi/4$. In our calculations, not variation of the refractive indexes with frequency was considered, neither imaginary part was taken into account which imply that dispersion and absorption are neglected. Note that in all our calculations the number n of local structural periods (where the director gives a full turn) remains constant with $n = 70$.

In our plots, T_{RR} (T_{LL}) represents right (left) copolarized transmittance, whereas the depolarized contribution or cross-polarized transmittance is given by T_{RL} (T_{LR}). Complementary, R_{RR} (R_{LL}) and R_{RL} (R_{LR}) are the corresponding reflectances in which their subscripts refer to the same meaning as that just explained for transmittances [33].

Before discussing the results, it is worth mentioning that the center wavelength, bandwidth, and edge wavelengths of the Bragg-type bands are given by Eqs. (23) and (24). At normal incidence, they give the spectral region for the Bragg-type band for a given magnitude of the DC applied electric field E_x . For normal incidence, tilt angle $\chi = \pi/4$, and no applied electric field, the edges of the optical band are given approximately by $\lambda_- = p_i\sqrt{2\epsilon_1\epsilon_3}/\sqrt{\epsilon_1 + \epsilon_3}$ ($\lambda_- = p_f\sqrt{2\epsilon_1\epsilon_3}/\sqrt{\epsilon_1 + \epsilon_3}$), and $\lambda_+ = p_f\sqrt{\epsilon_1}$ ($\lambda_+ = p_i\sqrt{\epsilon_1}$), when $p_i < p_f$ ($p_f < p_i$). The edges of the bands obtained by these latter expressions and Eqs. (23) and (24), agree with those obtained by means of our computational simulations for chiral photonic media with linear pitch gradients as well as for media with uniformly varying pitch.

Figure 2(a) shows the transmission T_{RR} and reflection R_{RR} spectra for circularly polarized light normally incident on a chiral structure with a linear pitch gradient, where the pitch rate of change is $\delta = 5.03 \times 10^{-3}$, the initial pitch is $p_i = 260$ nm and the final pitch is $p_f = p_{70} = 370$ nm. We observe a Bragg-type broadband, which is rippled and it broadens and enhances as the intensity of the applied DC electric field increases. We observe a stop transmission band and a reflection band with wavelength edges at $\lambda_- = 392$ nm and $\lambda_+ = 566$ nm, when there is no applied electric field, which are in

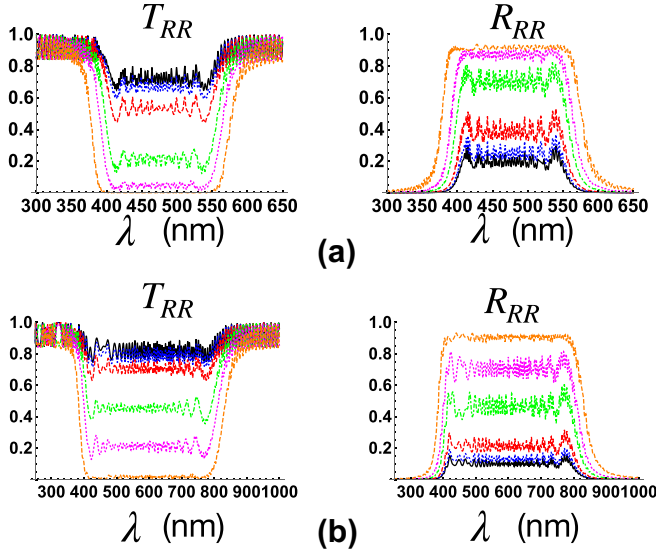


FIG. 2. Transmission spectra T_{RR} and reflection spectra R_{RR} for normal incidence of light on a SCM with linearly spatial varying pitch. The pitch at each point of the sample is $p(x) = p_0 + \delta x$, where x is the nonhomogeneity coordinate and for the local structural j period, the pitch at the end of the local period is $p_j = \frac{p_0}{(1-\delta)^j}$, $j = 1, \dots, n$. The number of local structural periods is $n = 70$. Low frequency (DC) electric field $E_x = 0$ (black solid line), $E_x = 0.5$ GV/m (blue dotted line), $E_x = 1$ GV/m (red dashed line), $E_x = 2$ GV/m (green dot-dashed line), $E_x = 3$ GV/m (magenta dotted line), $E_x = 5$ GV/m (orange dashed line) a) $\delta = 5.03 \times 10^{-3}$, the initial pitch is $p_i = p_0 = 260$ nm, the final pitch is $p_f = p_{70} = 370$ nm and $\Delta p = p_f - p_i = 110$ nm. (b) $\delta = 1.04 \times 10^{-2}$, the initial pitch is $p_i = p_0 = 260$ nm, the final pitch is $p_f = p_{70} = 540$ nm, and $\Delta p = 280$ nm. The refractive indexes are $n_1 = 1.530$, $n_3 = 1.483$, tilt $\chi = \pi/4$, the electro-optic coefficients $r_{41} = 24.5$ pm/V and $r_{63} = 8.5$ pm/V, all other electro-optic coefficients are zero, $r_{JK} = 0$, $J = 1, 2, \dots, 6$ and $K = 1, 2, 3$.

the violet-green region of the visible spectrum. Meanwhile, for an applied DC electric field $E_x = 5$ GV/m, the Bragg band edges are $\lambda_- = 376$ nm and $\lambda_+ = 587$ nm, thus, the optical band has broadened to the ultraviolet-yellow region of the visible spectrum. The optical reflection band covers a wide region of the visible spectrum, which means that the sample is iridescent [4].

Figure 2(b) plots the same thing as Fig. 2(a) but takes $\delta = 1.04 \times 10^{-2}$, $p_0 = 260$ nm, and $p_f = 540$ nm. The difference between the initial pitch p_0 and the final pitch p_f has increased (δ has increased for the given initial pitch) compared with the above case, which implies that the Bragg-type broadband gets wider. We observe the enhancement and broadening of the band as the intensity of the applied electric field increases. Here, the optical band gets wider than the visible spectrum under an applied DC electric field. For normal incidence, the wavelength edges of the Bragg band are at $\lambda_- = 392$ nm and $\lambda_+ = 826$ nm, when there is no applied electric field, which are in the violet-infrared region of the visible spectrum, while the optical band edges are $\lambda_- = 376$ nm and $\lambda_+ = 857$ nm, for an applied DC electric field $E_x = 5$ GV/m; thus, the optical band is in the ultraviolet-infrared region of the visible spectrum. Hence, the optical band covers a wider region than

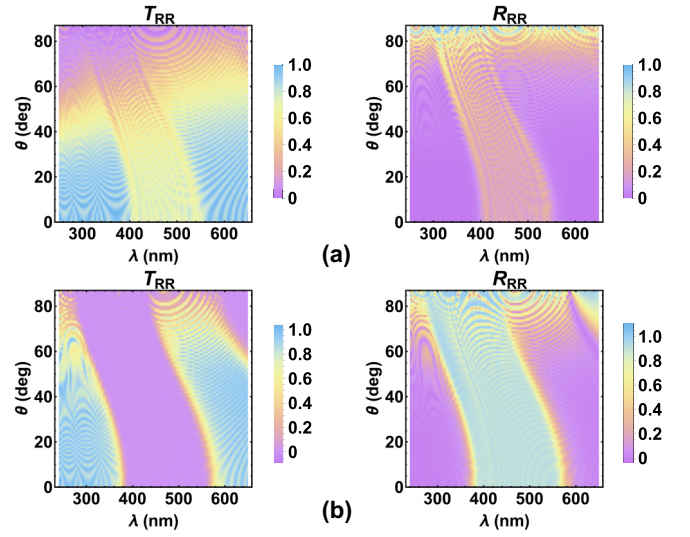


FIG. 3. Transmission T_{RR} and reflection R_{RR} spectra versus wavelength λ and angle of incidence of light, θ , for a chiral media with linear pitch gradient and the same medium parameters as for Fig. 2(a). $p_i = 260$ nm, $p_f = 370$ nm, and $\Delta p = 110$ nm. (a) No electric field is applied, $E_x = 0$ GV/m. (b) Low-frequency (DC) electric field, $E_x = 5$ GV/m.

the visible spectrum, which means that the sample looks silver [4–14].

Figure 3 exhibits transmission T_{RR} and reflection R_{RR} spectra versus wavelength λ and angle of incidence of light, θ , for circularly polarized light obliquely incident on a chiral medium with linearly spatial-varying pitch and the same parameters as for Fig. 2(a), where $p_i = 260$ nm and $p_f = 370$ nm, and the difference between the initial and final pitch is $\Delta p = 110$ nm. We observe the Bragg-type broadband, where the optical band blueshifts as the angle of incidence increases. Here, as in Fig. 2(a), at normal incidence of light and no applied electric field (black solid line), the optical band is located in the violet-green region of the visible spectrum [$\lambda \in (392, 566)$ nm, see Fig. 3(a)].

We observe that the Bragg-type broadband is widened and enhanced when a low-frequency (DC) electric field E_x is applied along the nonhomogeneity axis [see Fig. 3(b)]. At normal incidence for a low-frequency (DC) electric field $E_x = 5$ GV/m, the optical band is in the ultraviolet-yellow region of the visible spectrum [$\lambda \in (376, 587)$ nm, as in Fig. 2(a), orange dashed line], therefore, the Bragg optical band has broadened from the violet-green region to the ultraviolet-yellow region of the visible spectrum. We also observe the blueshift of the band when the angle of incidence grows.

Figure 4 depicts transmission T_{RR} and reflection R_{RR} spectra versus wavelength λ and angle of incidence, θ , of light, for circularly polarized light obliquely incident on a chiral medium with linearly spatial-varying pitch and the same parameters as for Fig. 2(b), where $p_i = 260$ nm and $p_f = 540$ nm, whereas the difference between the initial and final pitch, $\Delta p = 280$ nm, has increased (δ has increased for a given initial pitch). The Bragg broadband is displayed in transmission T_{RR} and reflection R_{RR} spectra and the band blueshifts as the angle of incidence increases. We observe

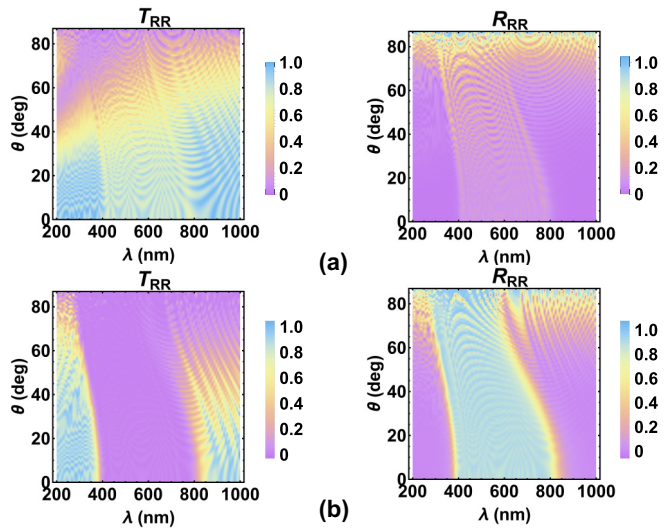


FIG. 4. Transmission T_{RR} and reflection R_{RR} spectra as a function of the wavelength λ and angle of incidence angle, θ , of electromagnetic waves for a chiral media with linear pitch gradient and the same medium parameters as for Fig. 2(b). $p_i = 260$ nm, $p_f = 540$ nm, $\Delta p = 280$ nm. (a) No electric field is applied, $E_x = 0$ GV/m. (b) Low-frequency (DC) electric field, $E_x = 5$ GV/m.

that the Bragg-type band has broadened compared with the band of the first case where $\Delta p = 110$ nm (see Fig. 3). For normal incidence of light and no applied electric field, the wavelength edges of the optical band are at $\lambda_- = 392$ nm and $\lambda_+ = 826$ nm, which are in the violet-infrared region of the visible spectrum [see Fig. 4(a)]. Moreover, the band is practically nonexistent when there is no electric field applied and is dramatically broadened and enhanced when a DC electric field is applied, as we discuss further below.

We observe in Fig. 4(b) that, when a low-frequency (DC) electric field is applied along the nonhomogeneity axis, where the magnitude is $E_x = 5$ GV/m, the practically absent Bragg-type optical band has completely developed. The optical band has broadened, compared with the band of the medium with no applied DC electric field. Here, the wavelength edges of the Bragg band are $\lambda_- = 376$ nm and $\lambda_+ = 857$ nm, hence, the optical band is in the ultraviolet-infrared region of the visible spectrum [as in Fig. 2(b), orange dashed line]. Thus, the Bragg optical band has widened from the violet-infrared region to the ultraviolet-infrared region of the electromagnetic spectrum, which implies that, under the electric field, the appearance of the sample is silver [4–14].

Heretofore, we have studied chiral media with linear pitch gradients, in the next example the SCM owns a uniformly varying pitch as depicted in Sec. II C. Below, we shall see that the spectra exhibit a similar behavior as that for the linear pitch gradient case.

Figure 5 presents transmission T_{RR} and reflection R_{RR} spectra versus wavelength λ and angle of incidence of light, θ , for circularly polarized light obliquely incident on a chiral medium with uniformly spatial-varying pitch, where the initial and final pitches in the chiral structure are $p_i = 345$ nm and $p_f = 665$ nm, and $\Delta p = 320$ nm. We observe that the Bragg-type band lies in the green-infrared region of the vis-

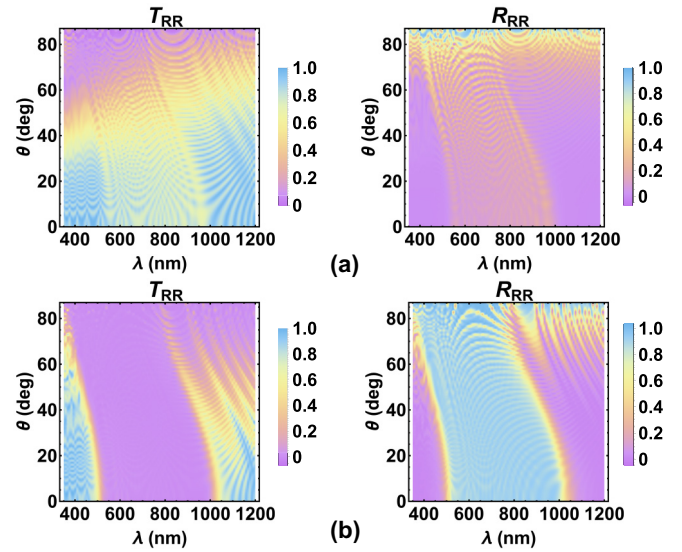


FIG. 5. Transmission T_{RR} and reflection R_{RR} spectra versus wavelength λ and angle of incidence of light, θ , for a chiral medium with uniformly spatial-varying pitch. Refractive indexes are $n_1 = 1.530$, $n_3 = 1.483$, tilt $\chi = \pi/4$, the electro-optic coefficients $r_{41} = 24.5$ pm/V and $r_{63} = 8.5$ pm/V, all other electro-optic coefficients are zero, $r_{JK} = 0$, $J = 1, 2, \dots, 6$, and $K = 1, 2, 3$; $p_i = p_1 = 345$ nm, $p_f = p_{70} = 665$ nm and $\Delta p = 320$ nm. (a) No electric field is applied, $E_x = 0$ GV/m. (b) Low-frequency (DC) electric field, $E_x = 5$ GV/m.

ible electromagnetic spectrum, $\lambda \in (520, 1018)$ nm, and it blueshifts as the angle of incidence increases.

Similar to the above case, the almost nonexistent optical band, for no applied electric field, widens and enhances when a DC electric field is applied along the nonhomogeneity axis, $E_x = 5$ GV/m [see Fig. 5(b)]. We observe that the Bragg band has broadened in the green-infrared region of the electromagnetic spectrum. Reflection in that region of the spectrum manifests as a golden appearance of the chiral structure [11].

Figures 6 and 7 display the remaining remittances (transmission T_{LL} , reflection R_{LL} , transmission T_{RL} , and reflection R_{RL}) for a chiral medium with uniformly varying pitch and the same medium parameters as for Fig. 5, when there is no applied electric field, and when the applied DC electric field is $E_x = 5$ GV/m, respectively. For no applied electric field, we observe typical spectra, when circularly polarized light impinges on a SCM, where incident left-circularly polarized (LCP) light is highly transmitted through the chiral medium as LCP light and there is no reflection of LCP light. Reflection of LCP light is only observed when light impinges almost perpendicular to the slab, while the transmission diminishes as the angle of incidence increases for angles $\theta \gtrsim 40^\circ$. In addition, LCP (RCP) light is mostly not transmitted or reflected as RCP (LCP) light (see Fig. 6).

On the other hand, when a DC electric field is applied, mainly the above-described overall behavior is observed. Note that the cross-polarized spectra show that, for LCP (RCP) incident light on the SCM with spatially varying pitch, the transmission as RCP (LCP) light diminishes, while partial reflection of RCP (LCP) light appears at some regions of angles of incidence, θ , and for wavelengths $\lambda > 800$ nm

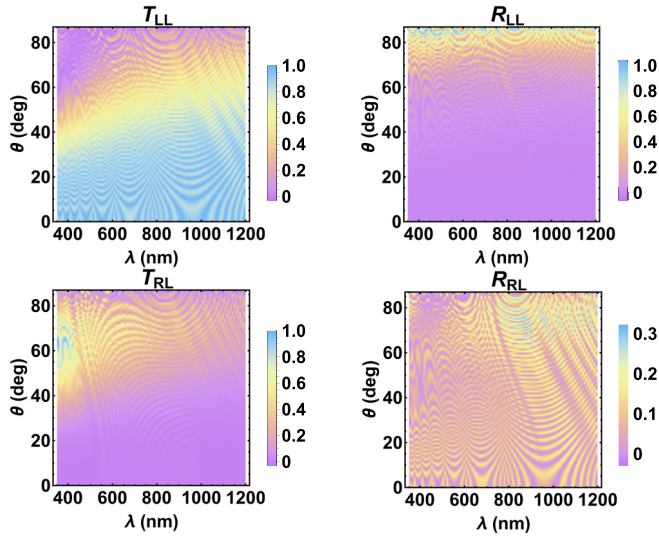


FIG. 6. Copolarized remittances: transmission T_{LL} and reflection R_{LL} ; cross-polarized remittances: transmission T_{RL} and reflection R_{RL} against wavelength λ and angle of incidence, θ , of electromagnetic waves for a chiral medium with uniformly varying pitch and the same medium parameters as for Fig. 5, where $p_i = 345$ nm, $p_f = 665$ nm, and $\Delta p = 320$ nm. No electric field is applied, $E_x = 0$ GV/m. $T_{RL} = T_{LR}$ and $R_{RL} = R_{LR}$ to numerical accuracy, so the plots of T_{LR} and R_{LR} are not displayed here.

(see Fig. 7), compared with the case where there is no applied electric field.

Further calculations that are not displayed in this study show that T_{LL} , R_{LL} , T_{RL} , and R_{RL} spectra have a similar be-

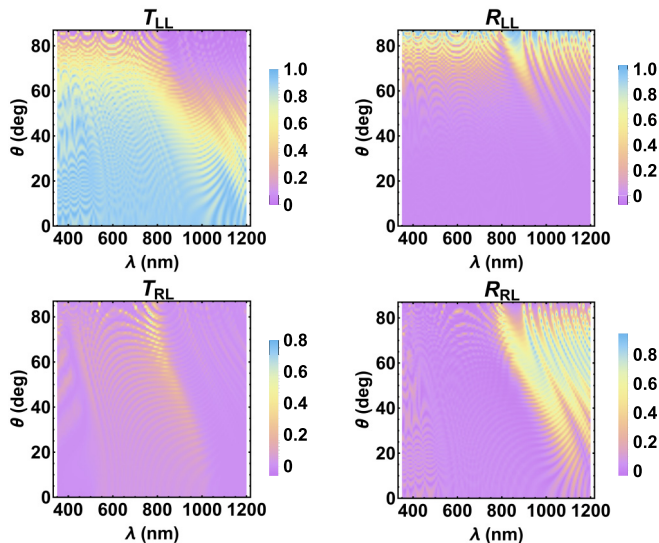


FIG. 7. Copolarized remittances: transmission T_{LL} and reflection R_{LL} ; cross-polarized remittances: transmission T_{RL} and reflection R_{RL} against wavelength λ and angle of incidence of light, θ , of electromagnetic waves for a chiral medium with uniformly varying pitch and the same medium parameters as for Fig. 5, where $p_i = 345$ nm, $p_f = 665$ nm, and $\Delta p = 320$ nm. A low-frequency electric field is applied, $E_x = 5$ GV/m. $T_{RL} = T_{LR}$ and $R_{RL} = R_{LR}$ to numerical accuracy, so the plots of T_{LR} and R_{LR} are not displayed here.

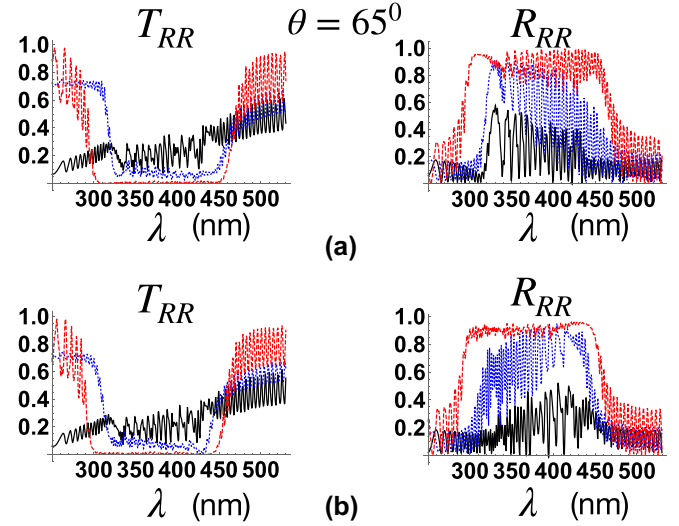


FIG. 8. Transmission T_{RR} and reflection R_{RR} spectra where the angle of incidence of light is $\theta = 65^\circ$ for a chiral media with linearly varying pitch and the same medium parameters as for Figs. 2(a) and 3: (a) $p_i = 260$ nm and $p_f = 370$ nm, $\Delta p = 110$ nm. (b) $p_i = 370$ nm and $p_f = 260$ nm, $\Delta p = 110$ nm. $E_x = 0$ GV/m (black solid line), $E_x = 2$ GV/m (blue dotted line), and $E_x = 5$ GV/m (red dashed line).

havior as described above for the other cases that we have considered here.

Notice that the transmission and reflection spectra fulfill conservation of energy, where $T_{RR} + R_{RR} + T_{RL} + R_{RL} = 1$ ($T_{LL} + R_{LL} + T_{LR} + R_{LR} = 1$, $T_{LL} \approx 1$, $R_{LL} \approx 0$), our calculations gives that $T_{RL} + R_{RL} \approx 0.1$, so $T_{RR} \approx 0.9 - R_{RR}$, with and without electric field, however, the reflection R_{RR} increases as the DC electric field increases, where $R_{RR} \approx 0.9$ in the optical band for an external electric field $E_x = 5$ GV/m, thus $T_{RR} \approx 0$ and we observe the enhancement of the optical band.

Below, in Figs. 8 and 9, we analyze changes of the transmission T_{RR} and reflection R_{RR} spectra for a particular oblique angle of incidence of light ($\theta = 65^\circ$) and different applied DC electric fields, when the pitch value increases and when it decreases in the chiral media, for linearly and uniformly varying pitch, respectively.

Figure 8 displays transmission T_{RR} and reflection R_{RR} spectra where the angle of incidence of light is $\theta = 65^\circ$ for [Fig. 8(a)] the case of increasing linear pitch gradient and [Fig. 8(b)] the case of decreasing linear pitch gradient (same edge pitches in the structure) for different DC electric-field amplitudes [the same material parameters as in Figs. 2(a) and 3]. We observe that the optical bands are in the same wavelength region for both cases and there are peaks and ripples in the spectra; when the pitch increases in the structure, the reflection amplitude is larger at shorter wavelengths. Meanwhile, for the case of decreasing pitch gradient, the reflection amplitude is larger at larger wavelengths. This means that the prevalent reflection colors at oblique incidence are to some extent different, depending whether the pitch increases or decreases in the chiral structure and depending on the angle of incidence of light and the magnitude of the applied

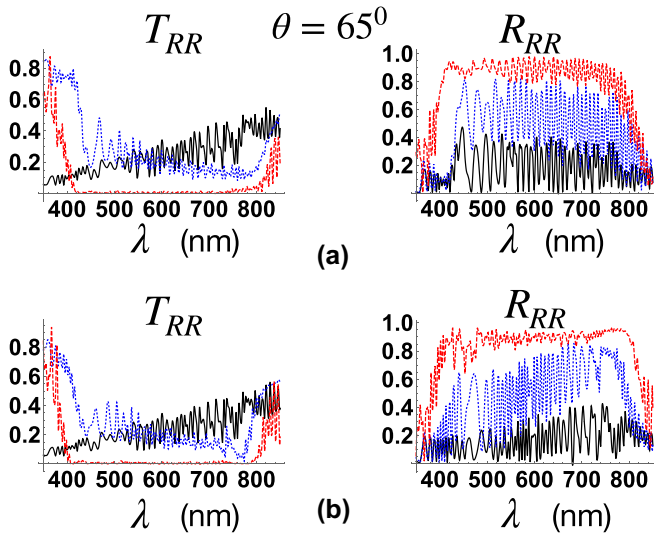


FIG. 9. Transmission T_{RR} and reflection R_{RR} spectra where the angle of incidence is $\theta = 65^\circ$ for a chiral media with uniformly varying pitch and medium parameters as for Fig. 5. (a) $p_i = 345$ nm, $p_f = 665$ nm, and $\Delta p = 320$ nm. (b) $p_i = 665$ nm and $p_f = 345$ nm, $\Delta p = 320$ nm. $E_x = 0$ GV/m (black solid line), $E_x = 2$ GV/m (blue dotted line), $E_x = 5$ GV/m (red dashed line).

electric field. In addition, the asymmetry, peaks, and ripples in the spectra tend to disappear as the DC electric amplitude increases.

Figure 9 displays transmission T_{RR} and reflection R_{RR} spectra for which the incidence angle of light is $\theta = 65^\circ$, for [Fig. 9(a)] the increasing uniformly spatial-varying pitch case and [Fig. 9(b)] the decreasing uniformly varying pitch case (same edge pitch values in the structure); for various DC electric field amplitudes (the same material parameters as for Fig. 5). We observe that the optical bands are in the same wavelength region for both cases while spectra display peaks and ripples. For the positive-pitch gradient case, the reflection amplitude is slightly larger at shorter wavelengths; meanwhile, when the pitch decreases in the chiral medium, the reflection amplitude is larger at larger wavelengths. This implies that the prevalent reflection colors at oblique incidence are slightly different, whether the pitch is increasing or decreasing in the chiral structure and depending on the angle of incidence of the light and the magnitude of the applied electric field. We point out that the asymmetry, peaks, and ripples in the spectra tend to be removed as the DC electric amplitude increases, as in Fig. 8.

Figure 10 shows circular dichroism (CD) as a function of the light wavelength λ . Figure 10(a) shows a SCM with linearly varying pitch for the same medium parameters as Fig. 4, and [Fig. 10(b)] for a SCM with uniformly varying pitch, for different values of DC electric field E_x . Here, circular dichroism is defined as $CD = \frac{T_{RR} - T_{LL}}{T_{RR} + T_{LL}}$. We observe a band for the circular dichroism for those wavelengths of the optical band. Since the circular dichroism depends on the difference of the transmission, $T_{RR} - T_{LL}$, and the transmission T_{RR} decreases from one to zero as the applied electric field increases and T_{LL} is approximately one, the CD decreases from zero to minus one as the DC electric field increases. Notice that the

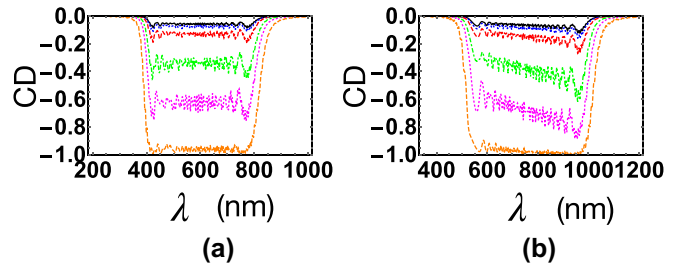


FIG. 10. Circular dichroism (CD) as a function of wavelength λ . (a) For a chiral medium with linearly varying pitch and the same medium parameters as for Figs. 2(b) and 4. (b) For a chiral medium with uniformly varying pitch and the same medium parameters as for Fig. 5. We considered different values of the low-frequency (DC) electric field, $E_x = 0$ (black solid line), $E_x = 0.5$ GV/m (blue dotted line), $E_x = 1$ GV/m (red dashed line), $E_x = 2$ GV/m (green dot-dashed line), $E_x = 3$ GV/m (magenta dotted line), $E_x = 5$ GV/m (orange dashed line).

circular dichroism is caused by the structural chirality, not by a distinct absorption for different circular polarization of light. Figure 10(b) displays the circular dichroism for the uniformly varying pitch sample, here the difference between the uniformly and the linearly varying pitch case is the asymmetry in the CD band for the uniformly varying pitch sample; the same that is observed in the Bragg band.

Figure 11 exhibits the CD depending on the light wavelength λ and the incident angle of light, θ . We observe the enhancement of the CD when the DC electric field is applied and the blueshift of the band as the incident angle increases.

A complementary property to characterize chiral systems was calculated at the end of Sec. II B where a generalization of the so-called optical activity for varying pitch media was proposed. Here, we calculate such a quantity for the first example [see Fig. 2(a)] that we analyze here. To evaluate Eq. (27) we need to calculate the central wavelength λ_0 as given by Eq. (23) which for the parameters used for the model of Fig. 2(a), we obtain $\lambda_0 = 479$ nm. Then, for an electric field $E_x = 1$ GV/m, we get, using Eq. (10), that $\epsilon_E = 0.126$. Hence, the optical activity gives rise to $\Upsilon_0/d = 10^5$ deg/cm², near the first edge of the optical band, which is about two

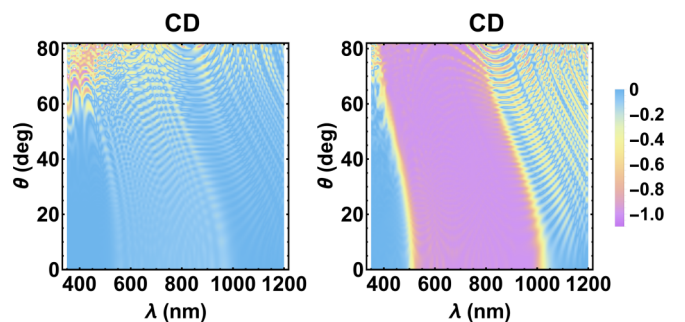


FIG. 11. Circular dichroism (CD) as a function of wavelength λ and angle of incidence of light, θ , for a chiral medium with uniformly varying pitch and the same medium parameters as Fig. 5. (a) No electric field is applied, $E_x = 0$ GV/m. (b) External applied DC electric field along the nonhomogeneity axis: $E_x = 5$ GV/m.

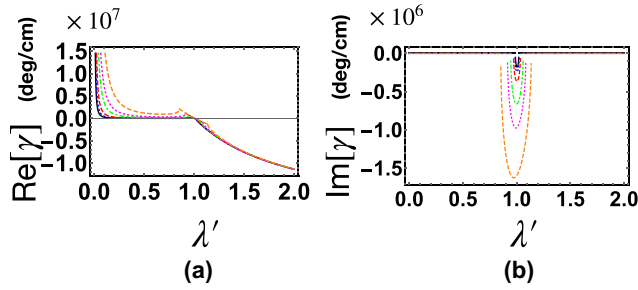


FIG. 12. (a) Real part of the optical activity per centimeter, $\text{Re}[\gamma]$, as a function of the dimensionless wavelength λ' , for a chiral medium with spatially varying pitch, where $\gamma = \Upsilon/d$, Υ is the optical activity and d is the thickness of the medium. (b) Imaginary part of the optical activity per centimeter, $\text{Im}[\gamma]$, as a function of the dimensionless wavelength λ' [same medium parameters as for Fig. 2(b)]. For different values of the low-frequency (DC) electric field: $E_x = 0$ (black solid line), $E_x = 0.5$ GV/m (blue dotted line), $E_x = 1$ GV/m (red dashed line), $E_x = 2$ GV/m (green dot-dashed line), $E_x = 3$ GV/m (magenta dotted line), $E_x = 5$ GV/m (orange dashed line).

orders of magnitude larger than that estimated in Sec. II B for a constant pitch structure; which is already an usual gigantic optical activity for SCM. As we mentioned there, the external field contributes to enlarge dramatically the rotatory power of the helical structure. Indeed, we can affirm that the Pockels effect, which affects the dielectric tensor by means of the electro-optic coefficients, is responsible for the widening and enhancement induced by the DC electric field of the optical band. In Fig. 12 we plot the real and imaginary parts of the normalized optical activity $\text{Re}[\gamma]$ ($\text{Im}[\gamma]$) versus the dimensionless wavelength λ' , parametrized by the DC external electric field without approximation [as given by Eq. (15)], where $\gamma = \Upsilon/d$, Υ is the optical activity, and d is the thickness of the medium. Figure 12(a) corresponds to the real part of γ , whereas Fig. 12(b) provides the corresponding imaginary part. This plot evinces the dramatic dependence of the rotatory power on the external field. As seen, both the magnitude of optical activity and bandwidth increase by enlarging the DC electric field. In this plot the band reflection region is delimited by the nondifferentiable points in the curves in which the imaginary part of γ is not vanishing. It should be mentioned that, for wavelengths longer than the characteristic wavelength $\lambda' = 1$, γ changes sign. Gigantic rotatory power and circular dichroism have been also measured and calculated for diverse plasmonic systems [35–38]. Those systems have the practical advantage of being constructed in very thin films, however, the relevance of our proposed SCM of varying pitch is that this exhibits extremely broadband reflection which, as discussed here, increases by applying the external electric field. Indeed, our calculations depicted in Figs. 10–12 display that by applying an external DC field, the dichroism and giant optical activity get larger in amplitude for an even larger wavelength interval.

It is worth to mention that, in Ref. [17], we found that, for normal incidence of light, optical spectra are in the same wavelength region for both cases: a chiral medium for which the pitch increases or decreases (provided the edge

pitch values are swapped for both structures). Further calculations, which are not reported in this paper, reveal that the Bragg regime remains in the same wavelength interval for all incidence angles of light; either the pitch increases or decreases. However, the reflection amplitude enlarges for shorter (longer) wavelengths (within the optical band) for the increasing (decreasing) pitch gradient case; as the angle of incidence of light grows.

The difference in spectra between the two different pitch gradients studied here, linear and uniform gradients, is that for a uniformly varying pitch, spectra show that for longer wavelengths the Bragg band is better defined than for shorter wavelengths, under no external applied electric field and with δ larger than one percent of the starting pitch [17]. It is because sections with larger local structural periods (periods with larger constant pitch values) cover a larger part of the structure, and their Bragg regimes overlap more extensively, which explains why the Bragg-type regime is better defined for longer wavelengths, corresponding to periods with the larger pitches in the structure. Moreover, for shorter-wavelength waves in the Bragg-type band, the transmission is larger, which is reasonable by noting that the longer wavelengths can only stand in sectors of the structure whose length is large enough to enter in the arrangement. Meanwhile, the shorter wavelengths can be propagated in all sectors: those with large and small periods. On the other hand, for SCM with a linear pitch gradient none of the periods with a particular pitch occupies larger regions in the medium and the sample is thinner compared with SCM with a uniformly varying pitch with the same number of local structural periods and initial and final pitch in the structure, then the optical band is nearly uniform for all wavelengths in the Bragg regime. Moreover, when an external DC electric field is applied, the asymmetry, peaks, and ripples in the optical bands tend to disappear; for SCM with either a uniform or linear pitch gradient.

IV. CONCLUSIONS

We studied optical spectra for circularly polarized light that obliquely impinges on a slab of a structurally chiral medium with either linear pitch gradients or uniformly varying pitches which locally possess a $42m$ point-group symmetry. We numerically compute the optical spectra by means of the piecewise uniform approximation of the transfer-matrix method. The considered chiral medium has a pitch that (a) linearly increases, or decreases, from an initial pitch at the beginning of the first local structural period to a final pitch at the end of the last period and (b) a pitch that uniformly increases or decreases in subsequent local structural periods.

For both pitch gradients, the optical spectra exhibit a Bragg broadband which is rippled and blueshifts as the angle of incidence of the light increases. The chiral structure has an initial and final pitch p_i and p_f , respectively, and the optical band covers from the Bragg band of a SCM with constant pitch p_i to the Bragg band of another SCM with constant pitch p_f . Moreover, the center wavelength and the bandwidth of the Bragg band are expressed in terms of the medium parameters and the magnitude of the applied DC electric field; where the wavelengths of the edges of the broadband are $\lambda_- = p_i \sqrt{2\epsilon_1 \epsilon_3} / \sqrt{\epsilon_1 + \epsilon_3}$ ($\lambda_+ = p_f \sqrt{2\epsilon_1 \epsilon_3} / \sqrt{\epsilon_1 + \epsilon_3}$) and

$\lambda_+ = p_f \sqrt{\epsilon_1}$ ($\lambda_+ = p_i \sqrt{\epsilon_1}$), when $p_i < p_f$ ($p_f < p_i$), at normal incidence for no applied electric field and tilt $\chi = \pi/4$. Notice that the edges of the optical bands obtained by these latter expressions and Eqs. (23) and (24), agree with those obtained by means of our computational simulations.

We found that the bandwidth broadens as the difference grows between the initial pitch p_i and the final pitch p_f (the pitch rate of change δ increases for a given initial pitch p_i). Besides, for a slab of chiral medium and varying pitch with no applied electric field, when the pitch difference in the chiral structure increases, the optical band tends to disappear. However, the Bragg band enhances, when an external low-frequency (DC) electric field is applied, and even when the optical band is practically imperceptible, it can be created, enhanced and broadened by enlarging the DC electric field.

In this study, we presented three examples of quite broad optical bands, where two of them cover a large region of the visible spectrum and the remaining one covers a wider region than that of the visible spectrum. Hence, the appearance of the media is iridescent, golden and silver, respectively. It is well known that iridescence is the result of reflection of light in either, different regions, or a very wide region of the visible electromagnetic spectrum; for instance, when the reflection is within the ultraviolet-green region of the electromagnetic spectrum. The golden color is the result of reflection in a region of light wavelengths from $\simeq 525$ to 1000 nm, i.e., from green to infrared. Meanwhile, a silver color medium reflects a wider interval than that of the visible spectrum, such that the eye is unable to perceive iridescence [4–14]. Indeed, these kinds of structural colors that are generated by reflection of light can be seen in nature in different insects, shells, and crustaceans.

The difference in spectra, regarding the two different pitch gradients studied here without an applied DC electric field is that for larger wavelengths, the Bragg band is better defined than for shorter wavelengths, for a uniformly varying pitch sample. However, the asymmetry in the Bragg bands of SCM with uniformly varying pitch disappears as the amplitude of the applied electric field increases. It is worth mentioning that the peaks and ripples exhibited in the optical bands are smoothed as the amplitude of the applied electric field gets larger.

In addition, for both (a) the increasing pitch gradient and (b) the decreasing pitch gradient cases (whenever the edge pitch values are swapped in the structure, either for linear or uniformly varying pitch), we found that the optical bands

are in the same wavelength interval, for all values of the angle of incidence of light. For either linear pitch gradients or uniformly varying pitch, optical spectra exhibit that at oblique incidence of light, for the increasing pitch gradient case, the reflection amplitude is larger (slightly larger for the uniform gradient) at shorter wavelengths, meanwhile for the decreasing pitch gradient case the reflection amplitude is larger at longer wavelengths. This asymmetry in the reflection band sharpens as the light incidence angle grows whereas it is smoothed when the amplitude of the applied electric field increases. This implies that the prevalent reflection colors at oblique incidence are slightly different whether the varying pitch is increasing or decreasing in the chiral structure and depending on the angle of incidence of light and the magnitude of the applied electric field.

Finally, we deduce an expression of the optical activity for chiral photonic media with variable pitch that depends on the material parameters. Besides, we found that the magnitude of the optical activity, circular dichroism and bandwidth increase by enlarging the DC electric field, which are related with the change in the refractive indexes of the electro-optic chiral medium under the external field.

We found that, even if the optical band is almost absent, a very broad band could be opened, by imposing a DC electric field; caused by corresponding electro-optic terms in the permittivity tensor elements, which are consistent with a great augmentation in both the optical activity and dichroism.

We expect that the study presented here motivates the fabrication of novel photonic devices, chiral photonic structures with a linear pitch gradient or a uniformly varying pitch, with possible applications such as circular polarization and wavelength-broadband filters, where the band can be broadened, enhanced, or even created by an external low-frequency (DC) electric field. Moreover, the photonic broadband can be selected in a specific region of the electromagnetic spectrum by choosing the material parameters, as well as the initial and final pitch in the structure. The method to fabricate SCM with varying pitch, we mainly suggest, is physical vapor deposition, although it is not restricted to this fabrication technique.

ACKNOWLEDGMENT

J. Adrian Reyes acknowledges financial support from the grant of Dirección General de Asuntos del Personal Académico, Universidad Nacional Autónoma de México (IN100921), Mexico.

-
- [1] P. G. de Gennes and J. Prost, *The Physics of Liquid Crystals* (Clarendon Press, Oxford, 1993).
 - [2] K. Robbie, M. J. Brett, and A. Lakhtakia, *Nature (London)* **384**, 616 (1996).
 - [3] M. Warner and E. M. Terentjev, *Liquid Crystal Elastomers* (Clarendon Press, Oxford, 2003).
 - [4] S. Berthier, *Iridescences* (Springer, New York, 2007).
 - [5] M. Mitov, *Soft Matter* **13**, 4176 (2017).
 - [6] D. Raabe, C. Sachs, and P. Romano, *Acta Mater.* **53**, 4281 (2005).
 - [7] D. Raabe, P. Romano, C. Sachs, A. Al-Sawalmih, H. G. Brokmeier, S. B. Yi, G. Servos, and H. G. Hartwig, *J. Cryst. Growth* **283**, 1 (2005).
 - [8] P. Romano, H. Fabritius, and D. Raabe, *Acta Biomater.* **3**, 301 (2007).
 - [9] S. Nikolov, M. Petrov, L. Lymperakis, M. Friak, C. Sachs, H. O. Fabritius, D. Raabe, and J. Neugebauer, *Adv. Mater.* **22**, 519 (2010).
 - [10] T. Lenau and M. Barfoed, *Adv. Eng. Mater.* **10**, 299 (2008).

- [11] W. E. Vargas, E. Avendano, M. Hernández-Jiménez, D. E. Azofeifa, E. Libby, A. Solís, and C. Barboza-Aguilar, *Biomimetics* **3**, 30 (2018).
- [12] A. E. Seago, P. Brady, J. P. Vigneron, and T. D. Schultz, *J. R. Soc. Interface* **6**, S165 (2009).
- [13] M. Srinivasarao, M. Crne, V. Sharma, and J. O. Park, *Yearbook of Science and Technology* (McGraw-Hill, New York, 2011).
- [14] H. Arwin, R. Magnusson, J. Landin, and K. Järrendahl, *Philos. Mag.* **92**, 1583 (2012).
- [15] A. Mendoza-Galván, K. Järrendahl, and H. Arwin, *J. Opt.* **21**, 125401 (2019).
- [16] A. Mendoza-Galván, L. Fernández del Río, K. Järrendahl, and H. Arwin, *Sci. Rep.* **8**, 6456 (2018).
- [17] L. O. Palomares and J. A. Reyes, *J. Phys.: Condens. Matter* **32**, 175303 (2020).
- [18] M. Jeong and K. Kwak, *IEEE Photon. J.* **11**, 4700211 (2019).
- [19] H. Lu, C. Wei, Q. Zhang, M. Xu, Y. Ding, G. Zhang, J. Zhu, K. Xie, X. Zhang, Z. Hu, and L. Qiu, *Photon. Res.* **7**, 137 (2019).
- [20] M. Mitov, A. Boudet, and P. Sopéna, *Eur. Phys. J. B* **8**, 327 (1999).
- [21] A. Boudet, C. Binet, M. Mitov, C. Bourgerette, and E. Boucher, *Eur. Phys. J. E: Soft Matter Biol. Phys.* **2**, 247 (2000).
- [22] C. Binet, M. Mitov, and A. Boudet, *Mol. Cryst. Liq. Cryst. Sci. Technol. Sect. A* **339**, 111 (2000).
- [23] Q. Chen, S. Wang, H. Gao, J. Zhang, Y. Xing, Z. Yang, H. Cao, and W. He, *Liq. Cryst.* **46**, 952 (2019).
- [24] A. Lakhtakia and R. Messier, *Sculptured Thin Films* (SPIE Press, Bellingham, 2005).
- [25] J. D. Lin, H. Y. Lin, G. J. Wei, Y. C. Chuang, L. J. Chen, T. S. Mo, and C. R. Lee, *J. Mater. Chem. C* **7**, 4740 (2019).
- [26] E. P. A. Van Heeswijk, J. J. H. Kloos, N. Grossiord, and A. P. H. J. Schenning, *J. Mater. Chem. A* **7**, 6113 (2019).
- [27] M. Rafayelyan, G. Agez, and E. Brasselet, *Phys. Rev. A* **96**, 043862 (2017).
- [28] Y. S. Zhang, A. V. Emelyanenko, and J. H. J. Liu, *J. Polym. Sci. Part B: Polym. Phys.* **55**, 1427 (2017).
- [29] A. Lakhtakia and J. A. Reyes, *Optik* **119**, 253 (2008).
- [30] J. D. Jackson, *Classical Electromagnetics* (Wiley, New York, 1999).
- [31] J. A. Reyes and A. Lakhtakia, *Opt. Commun.* **266**, 565 (2006).
- [32] R. W. Boyd, *Nonlinear Optics* (Academic Press, New York, 1992).
- [33] We will take electric fields of the order of $\text{kV}/\mu\text{m}$. Fields even larger has been used within the picture tube of a TV set [34].
- [34] M. Mandl, *Mandl's Television Servicing* (McMillan Company, New York, 1972), p. 58.
- [35] R. Knipper, T. G. Mayerhöfer, V. Kopecky Jr., U. Huebner, and J. Popp, *ACS Photon.* **55**, 1176 (2018).
- [36] G. Pellegrini, M. Finazzi, M. Celebrano, L. Duò, and P. Biagion, *Chirality* **30**, 883 (2018).
- [37] A. V. Kondratov, M. V. Gorkunov, A. N. Darinskii, R. V. Gainutdinov, O. Y. Rogov, A. A. Ezhov, and V. V. Artemov, *Phys. Rev. B* **93**, 195418 (2016).
- [38] O. V. Kotov and Yu. E. Lozovik, *Phys. Rev. B* **96**, 235403 (2017).